Geomechanics and Engineering, *Vol. 34, No. 5 (2023) 529-545*
https://doi.org/10.12989/gae.2023.34.5.529

Analytical model of isolated bridges considering soil-pile-structure interaction for moderate earthquakes

Mohammad Shamsi[1a], Ehsan Moshtagh*[2] and Amir H. Vakili[3,4b]

[1]*Department of Civil Engineering, University of Hormozgan, Bandar Abbas, Iran*
[2]*Department of Civil Engineering, University of Garmsar, Garmsar, Iran*
[3]*Department of Environmental and Civil Engineering, Faculty of Engineering, Karabuk University, Karabuk, 78050, Turkey*
[4]*Department of Civil Engineering, Zand Institute of Higher Education, Shiraz, Iran*

(*Received March 13, 2023, Revised July 24, 2023, Accepted July 31, 2023*)

Abstract. The coupled soil-pile-structure seismic response is recently in the spotlight of researchers because of its extensive applications in the different fields of engineering such as bridges, offshore platforms, wind turbines, and buildings. In this paper, a simple analytical model is developed to evaluate the dynamic performance of seismically isolated bridges considering triple interactions of soil, piles, and bridges simultaneously. Novel expressions are proposed to present the dynamic behavior of pile groups in inhomogeneous soils with various shear modulus along with depth. Both cohesive and cohesionless soil deposits can be simulated by this analytical model with a generalized function of varied shear modulus along the soil depth belonging to an inhomogeneous stratum. The methodology is discussed in detail and validated by rigorous dynamic solution of 3D continuum modeling, and time history analysis of centrifuge tests. The proposed analytical model accuracy is guaranteed by the acceptable agreement between the experimental/numerical and analytical results. A comparison of the proposed linear model results with nonlinear centrifuge tests showed that during moderate (frequent) earthquakes the relative differences in responses of the superstructure and the pile cap can be ignored. However, during strong excitations, the response calculated in the linear time history analysis is always lower than the real conditions with the nonlinear behavior of the soil-pile-bridge system. The current simple and efficient method provides the accuracy and the least computational costs in comparison to the full three-dimensional analyses.

Keywords: bridges; dynamic response; inhomogeneous soils; pile group; soil-structure interaction

1. Introduction

Structural responses to the earthquake excitations are representing the collective responses of the system consisting of the structure, the foundation (even the pile group), and the ground (the surrounding and underlying soil). The soil-structure interaction (SSI) is an engineering term that is considered the reciprocal effects of each part of this system to present a global collective response. Indeed, the dynamic SSI is the concept of considering the aforementioned mutual effects in the analytical or numerical formulation, modeling, and simulation (Limkatanyu *et al.* 2023, Shabani *et al*. 2021a, Shamsi *et al.* 2022). SSI influences can be either supportive or destructive to the structural performance depending on the specifications of structure, foundation, and soil (Jalili *et al.* 2023, Mylonakis and Gazetas 2000, Shabani *et al.* 2021b).

It can be inferred that the seismic behavior and vulnerability of structures with several mechanisms may be affected by SSI, significantly (Elchiti *et al.* 2023, Shamsi *et al.* 2022). Therefore, the investigation of the SSI phenomenon is inevitable in the seismic analysis of structures.

In the SSI process, the inertial interaction and kinematic interaction should be considered to reflect the real collective behavior of structures (Santisi d'Avila and Lopez-Caballero 2018, Mohammad *et al.* 2021, Wolf 1985). Displacements and rotations in the SSI system induced by the vibrating superstructure cause inertial interactions, while the stiff foundation elements cause the footing motions (due to the propagation of the seismic waves through the soil-pile system) to deviate from free-field motions, called kinematic interaction (Nikolaou *et al.* 2001, Wolf 1985). Base-slab averaging and embedment effects cause these deviations and impose the spatially variable displacement field. In the case of pile-supported foundations, the motions of foundation-level at the structure base can be further modified since piles interact with the propagated wave below the base slab (Di Laora *et al.* 2013, Di Laora and Rovithis 2015). That displacement field will then generate moment and shear along the pile. These two phenomena occur simultaneously and during the wave propagation, additional forces on pile foundations are induced by the surrounding soil lateral vibrations (kinematic interaction) along with the imposed forces caused by the superstructure

*Corresponding author, Assistant Professor
E-mail: e.moshtagh@fmgarmsar.ac.ir
[a]Assistant Professor
E-mail: mohamad.shamsi70@gmail.com
[b]Assistant Professor
E-mail: amirhoseinvakili@gmail.com

ISSN: 2005-307X (Print), 2092-6219 (Online)

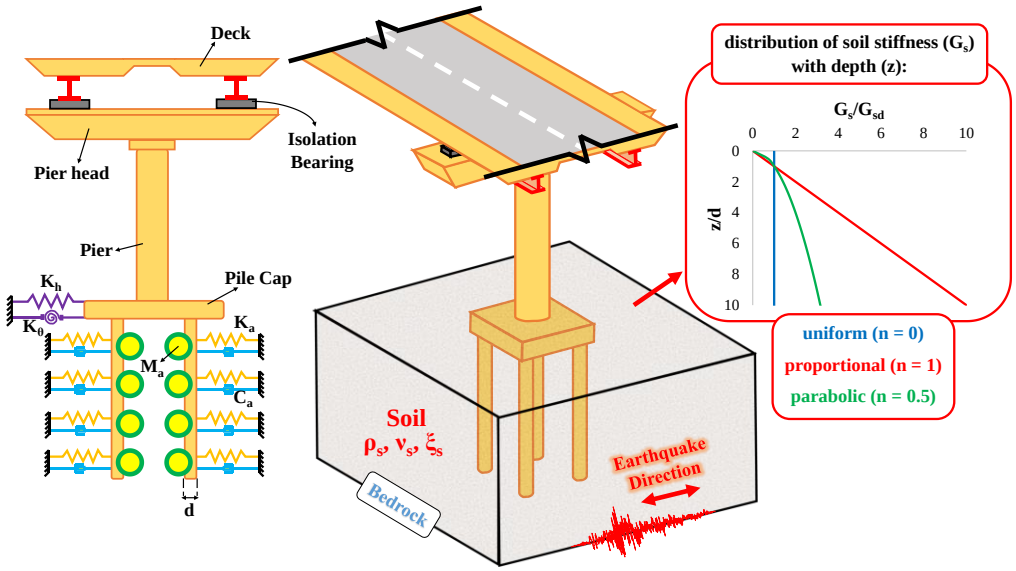

Fig. 1 Schematic model of the inhomogeneous soil-pile group-isolated bridge

vibrations (inertial interaction). Due to these effects, both inertial and kinematic forces must be considered in the designing process (Di Laora and Rovithis 2015, Shamsi and Ghanbari 2020).

Many researchers attempt to assert the significance of SSI effects on the seismic responses of bridges. For example, in 1992, Spyrakos showed how the consideration of SSI in the designing process of bridges leads to the reduction of their construction costs which can be interpreted by increasing structural period and displacement or decreasing base shear due to the SSI effects (Spyrakos 1990, 1992). It can be inferred that the bridge's performance and behavior will be changed and its design and seismic vulnerability scenario will be affected by the SSI (Kapasakalis *et al.* 2020, Massumi and Moshtagh 2013, Xiong *et al.* 2016).

One of the most impressive technologies for earthquake resistance systems is the base isolation technique. Rubber bearings, utilized for seismic isolation, provide large hysteretic damping and offer high seismic performance, economic saving, and thermal effects control (Kunde and Jangid 2006). Base isolation has been utilized to reduce the seismic vulnerability of bridges, as essential structures, by appealing to period elongation and dissipating the seismic energy (Mantakas *et al*. 2022, 2023). The impacts of soil stiffness are important in the isolated bridge's design (Antoniadis *et al.* 2019, Kapasakalis *et al.* 2021, Ucak and Tsopelas 2008). A stiff isolation system of bridges is usually affected severely by SSI effects while a flexible isolation system is not affected dramatically (Tongaonkar and Jangid 2003). Therefore, considering SSI effects for isolated bridges is meaningful.

Offering an analytical model in engineering problems is a fulcrum for developing numerical solutions for complicated problems. Besides, analytical solutions with their specifications such as accuracy, minimum computational cost, simplicity, and efficiency are benchmarks whenever experimental results are out of access. Developing an analytical model and offering its solution is a platform for understanding physical phenomena among researchers, however, it is not an easy task. Therefore, many analytical models were presented for the bridge-foundation interaction encompassing some limitations described as follows:

1) The foundations of heavy bridges are usually equipped with pile groups because of their weak soil bed properties, while most researchers have studied analytical models of these systems with a single pile foundation (Haouari and Bouafia 2023, Kampitsis *et al*. 2013, Kapasakalis *et al*. 2018, Maravas *et al*. 2014, Rovithis *et al.* 2011). For instance, Rovithis *et al.* (2011), Kampitsis *et al.* (2013), and Maravas *et al.* (2014) investigated the different structures resting on a single pile. Therefore, considering soil-pile groups-structure interactions in which less attention has been attracted is necessary to study analytically the isolated bridges equipped with piles.

2) For the sake of convenience, some studies presented simplified models of foundation-bridge interaction without any validation or verification to examine the seismic performance of bridges (González *et al*. 2019, 2020, Kapasakalis *et al.* 2018, Saitoh 2012, Spyrakos 1992). For instance, Spyrakos (1992) and González *et al.* (2020) presented three degrees of freedom (DOFs) analytical models which are too simplistic to consider the complicated SSI problem.

3) The semi-coupled substructuring method is the most common method to collect kinematic and inertial responses of bridges (Carbonari *et al.* 2017, González *et al.* 2020, Lesgidis *et al*. 2018). It separates the bridge system into two subsystems including the superstructure and the substructure. Also, final results were provided based on the superposition of kinematic and inertial response. Shear forces of the pier base, bending moments, and top deflections of the pier are overestimated in the substructuring method and the misprediction of spectral response is seen compared to the fully-coupled continuum modeling approach and field data (Rahmani *et al.* 2016).

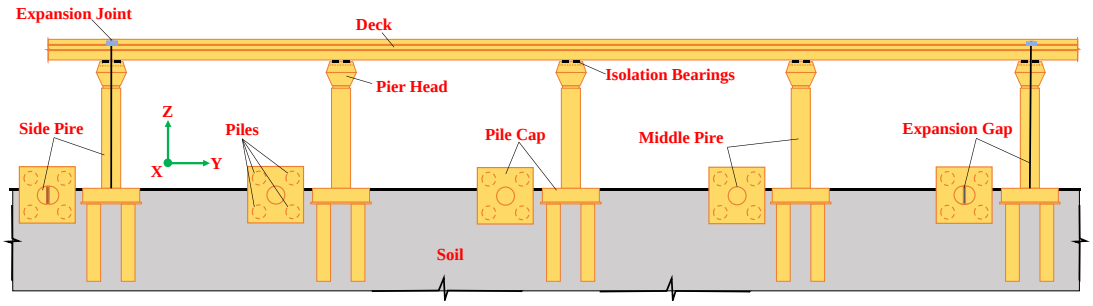

Fig. 2 Typical single-pier isolated bridges with the pile foundation

4) In most previous studies, SSI effects have been evaluated on the homogeneous soil profiles while soil deposits are usually nonhomogeneous (the shear modulus changes along with the depth). Usually, structures are constructed on layered alluviums and the fundamental period of structures is affected by this kind of inhomogeneity (Amornfa *et al.* 2023, Medina *et al*. 2019).

To the best of our knowledge, there are not any analytical coupled models for isolated bridges on inhomogeneous soil. However, the properties of the surrounding soil of piles have significant effects on their seismic performance.

Therefore, in this study, the triple interactions of inhomogeneous soil, pile group, and the isolated bridge are simultaneously investigated during frequent, low-acceleration amplitude, earthquakes (Fig. 1) by an accurate and comprehensive analytical model. Actually, an analytical model has been proposed to consider the soil-pile structure interaction (SPSI) effects on the seismic assessment of bridges. Assumptions related to each of the components, the main parameters of soil-pile elements, and the assembling process of the proposed model were provided in section 2. Sections 3-5 check the accuracy of the model in different situations considering modal and dynamic analyses. The analytical model presenting an isolated bridge system with limited DOFs equipped to the pile group evaluates SPSI effects with time history analyses. This model can be directly utilized for piles surrounded by layered homogenous and inhomogeneous soils. To discuss wave propagation analytically in a medium with layered structures in detail, refer to the other authors' papers (Moshtagh *et al.* 2019, Moshtagh *et al*. 2017, 2018). The proposed model outputs are compared with the results of centrifuge tests and fully three-dimensional (3D) continuum finite element models.

2. Analytical model

The current study investigates the seismic response of isolated bridges located on the pile foundations, utilizing a simplified model to consider the SSI phenomenon as shown in Fig. 2.

2.1 Assumptions

The main assumptions governing the problem in the proposed analytical model based on the following specifications without the loss of generality are stated below.

2.1.1 Superstructure components

This analytical model reflects the transverse (X direction) response of single-pier bridges consisting of multi-span simply supported decks. These bridges are usually constructed segment by segment (Fig. 2). These are separated by suitable expansion joints that guaranteed the independent seismic performance of each segment in the transverse direction (Ju 2013, Shamsi and Ghanbari 2020). Therefore, an analytical model of an independent segment can represent the collective manner of single-pier bridges.

The total DOF number can be decreased by the proposed analytical model considering the rigidity of the pile cap, pier head, and deck (Fig. 3). Also, considering the material and geometrical properties of piles and piers convinced us to model these parts of the system with the help of Euler–Bernoulli beam theory. Therefore, the problem can be simulated by an in-plan system with seven DOFs as illustrated in Fig. 3. This feature is available in the proposed model to consider more soil-pile elements for increasing the accuracy of results if it is necessary. The vertical DOF is decoupled from the rotational and horizontal ones and it is not included in the formulations if the in-plane response of the soil-foundation-pier system is considered. Thus, the main soil-foundation matrix arrays are the horizontal, rotational, and coupled roto-translational terms, presented in the analytical model (Fig. 3). M_d, M_{ph}, and M_{cap} denote the masses of the bridge deck, the pier head, and the pile cap, respectively. I_d, I_{ph}, and I_{cap} represent the mass moments of inertia of the bridge deck, the pier head, and the pile cap, respectively. $\bar{m}_{pier}$ and $\bar{m}_{pile}$ denote the masses per unit length of the pier and the pile, respectively. b and a are the thickness, and the width of the pile cap, while d, L, and h denote pile diameter, the length of the pile element, and the distance of the pier head mass centroid to the pile cap, respectively. For all materials, ρ and E are mass density and modulus of elasticity, respectively.

A high-damping rubber bearing (HDRB) isolator is utilized. HDRBs are common and adopted isolators in isolated bridges. A linear-viscose model can be assumed for HDRB and its weight can be neglected in comparison to the deck and the cap of pile masses (Matsagar and Jangid 2008). The HDRB linear stiffness in the X direction (K_{xb}) can be calculated as Eq. (1)

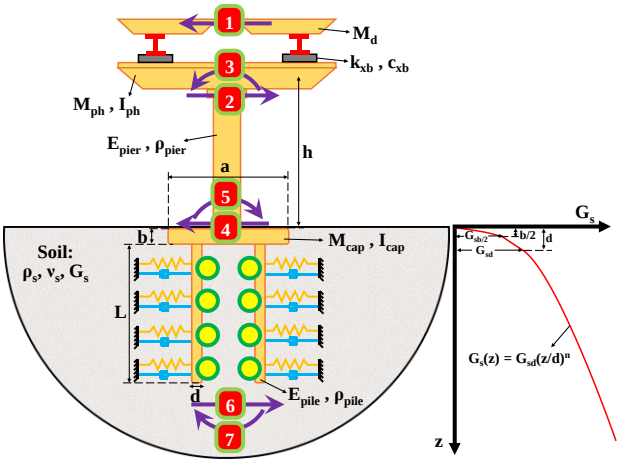

Fig. 3 Proposed example of the analytical model for the inhomogeneous soil-pile group-isolated bridge with 7 DOFs

$$K_{xb} = \frac{G_b bl}{h} \tag{1}$$

Where l, h, and b respectively denote the length, thickness, and width of the HDRB with the shear modulus of G_b. These isolators exhibit horizontal flexibility accompanied by high vertical stiffness.

The damping and stiffness demands have been supplied by setting the isolator period (T_b) to the specific values as Eq. (2)

$$T_b = 2\pi\sqrt{M_d / \sum K_{xb}} \tag{2}$$

The total effective viscous damping coefficient of the isolation system (ΣC_{bx}) was determined by Eq. (3) and the damping ratio of the isolator (β_{eff}) was assumed to be 10%.

$$\sum C_{xb} = \frac{4\pi M_d \beta_{eff}}{T_b} \tag{3}$$

For more details, the readers are referred to (AASHTO 1997) and (Shamsi and Ghanbari 2020).

2.1.2 Excitations

In this study, we focused on the frequent earthquakes and consequently low or moderate acceleration amplitude of excitations since the isotropic linear behavior is considered for the piles, pier, and soil. This condition is out of access in the case of rare earthquakes with intensive acceleration amplitude in which the nonlinear soil behavior and structural plastic characteristics are revealed. However, the proposed model needs to be modified in the case of severe earthquakes; this is being done in another research project. The accuracy and the deviation of analytical results in the case of severe earthquakes have been evaluated in Section 3 for this model. Earthquake excitations have been applied only in the transverse direction (X), which results in larger deflections of the bridge. The bending resistance of piers in this direction is weaker than that in other directions according to the formal design of typical bridges. All pier's excitations are similar. A synchronous seismic motion at all supports is assumed and non-uniform seismic excitations due to the effects of spatially varying earthquake ground motion (Elgamal *et al.* 2008, Qiu *et al.* 2020) are out of the scope of this study.

2.1.3 Soil domain

The soil is considered a continuum medium. The pile and soil are assumed with a perfect bonding (without any gap or slippage) at their interfaces. Also, the dynamic equilibrium condition of this system is derived from the D'Alembert principle. Soil mass density (ρ_s), hysteretic damping ratio (ξ_s), and Poisson's ratio (v_s) are assumed constant along with the depth (z), while the shear modulus (G_s) is a function of z represented by the generalized power-law function as Eq. (4)

$$G_s(z) = G_{sd}(z/d)^n \rightarrow$$

$$\text{Uniform } (n=0) \rightarrow \quad G_s(z) = G_{sd} = \overline{G}$$

$$\text{Proportional } (n=1) \rightarrow \quad G_s(z) = (G_{sd}/d).z = S.z \tag{4}$$

$$\text{Parabolic } (n=0.5) \rightarrow \quad G_s(z) = G_{sd}\sqrt{z/d}$$

where n is a dimensionless inhomogeneity factor, G_{sd} is the shear modulus at the depth of soil equal to the pile diameter ($z = d$) and S is representing the intensity of shear modulus variations along with the soil depth. Also, a similar function with reference to soil elastic modulus was approved by (Karatzia and Mylonakis 2012) and (Di Laora and Rovithis 2015) for certain values of n. For instance, the homogeneous medium (uniform soil profile) is modeled with n = 0, while for n = 1 a Gibson-type soil)Gibson 1974(, i.e. Proportional soil profile, is obtained. It should be noted that moderately overconsolidated and soft cohesive soils are generally associated with n = 1 and cohesionless soils are modeled with n < 1 (Di Laora and Rovithis 2015).

In the current study, the value of n is considered equal to 0.5, although the following equations can be extracted for any value of n. $G_s(z)$ profile which is normalized by the shear modulus of the nonhomogeneous soil at the depth equal to the pile diameter (G_{sd}) is shown in Fig. 1, corresponding to a uniform (n = 0), a proportional (n = 1), and a parabolic (n = 0.5) distribution of stiffness along with the soil depth.

2.1.4 Pile cap modeling

The series of closed-form formulations to estimate the spring coefficients are extracted by Gazetas for different foundation types and soil conditions (Gazetas 1991). In the following, e.g., Eqs. (5)-(7), the stiffness of the pile cap with the related coefficients for the case of a circular rigid surface foundation is presented

$$k_{Cap} = \begin{bmatrix} k_h & k_{h\theta} \\ k_{\theta h} & k_\theta \end{bmatrix} \tag{5}$$

where

$$k_h = \frac{8G_{sb/2}r_1}{2-\nu_s}$$

$$k_{h\theta} = k_{\theta h} = \frac{0.56G_{sb/2}r_1^{\,2}}{2-\nu_s} \tag{6}$$

$$k_\theta = \frac{8G_{sb/2}r_2^{\,3}}{3(1-\nu_s)}$$

b denotes the cap thickness, and $G_{sb/2}$ denotes the soil shear modulus in the soil depth equal to half of the footing thickness respectively. Also, r is the radius of the equivalent circular cap in the case of a square cap ($a \times a$) as follows

$$r_1 = \frac{a}{\sqrt{\pi}}$$

$$r_2 = \frac{a}{(3\pi)^{0.25}} \tag{7}$$

2.2 Main parameters of soil-pile elements

In this section, the calculation of parameters that are utilized in the proposed model is demonstrated. The mass, stiffness, and damping constants of the soil are connected to the pile as shown in Fig. 1 (M_a, K_a, and C_a, respectively). The procedure of soil-pile element formation with the help of virtual work theory and assembling sub-elements with the finite element method is expressed in the following.

2.2.1 Calculation of M_a, K_a, and C_a

Based on the linear elasticity and in the case of harmonic vibration, the dynamic stiffness of piles is presented by Novak with an approximate analytical expression (Novak 1974). This expression is proposed for the layered soil consisting of a series of independent horizontal layers with small thicknesses in a plane strain condition with small displacements. Each layer is homogeneous and isotropic with linear elastic behavior. The vertical cylindrical pile is assumed as a rigid body with perfect bonding to the soil; which is consistent with the theory of the Navier-Bernoulli beam. Later, this is extended to the viscoelastic materials for the case of frequency-independent material damping (Novak and Aboul-Ella 1978). The system damping was defined using a complex shear modulus of $G^* = G_s + i\,G'_s = G_s(1 + i\,D)$ in which D is the loss factor and considered as a function of γ (loss angle) as Eq. (8)

$$D = \tan\gamma = \frac{G'_S}{G_S} \tag{8}$$

G'_s and G_s denote the imaginary and real parts of the soil shear modulus, respectively. Finally, the complex horizontal stiffness for the soil, K_u, is given by Eqs. (9) and (10).

$$K_u = G\pi f(a_0, \nu, D) \tag{9}$$

where

$$f(a_0,\nu,D) = -a_0^{\,2}\frac{\begin{bmatrix}4K_1(b^*_0)K_1(a^*_0)\\ +a^*_0K_1(b^*_0)K_0(a^*_0)\\ +b^*_0K_0(b^*_0)K_1(a^*_0)\end{bmatrix}}{\begin{bmatrix}b^*_0K_0(b^*_0)K_1(a^*_0)\\ +a^*_0K_1(b^*_0)K_0(a^*_0)\\ +b^*_0a^*_0K_0(b^*_0)K_0(a^*_0)\end{bmatrix}}$$

$$a_0 = \omega d / 2V_s$$

$$a^*_0 = a_0 i / \sqrt{(1+iD)} \tag{10}$$

$$b^*_0 = b^*_0 / \chi$$

$$\chi = \sqrt{2(1-\nu_s)/(1-2\nu_s)}$$

in which K_i is the second kind of modified Bessel function and of order i (= 0,1), a_0 is a dimensionless frequency, ω is the vibration frequency (rad/s), V_s is the shear wave velocity of the soil, and ν_s is the soil Poisson's ratio. The 3D model of the soil-pile system during the lateral vibrations can be simplified to a 2D model in which the beam elements are applied to present the piles and number of linear springs with an assigned dynamic stiffness of K_u to present the soil behavior, as schematically illustrated in Fig. 4(a).

Also, a system of a single DOF (SDOF) with a rigid body was presented by Pacheco *et al.* (2008) as shown in Fig. 4(b). The mass (M) of the rigid body is constrained along one axis to move and is connected to a fixed point by a dashpot of constant C and spring with stiffness K. The impedance or dynamic stiffness $K_d(\omega)$ is the amplitude of the harmonic force with the frequency ω ($F(t)=K_d(\omega)\,e^{i\omega t}$) that should be applied to an SDOF model to have a unit steady-state harmonic displacement with frequency ω ($X(t) = 1e^{i\omega t}$). Expressing the impedance of the SDOF model is straightforward as Eq. (11)

$$K_d(\omega) = K - \omega^2 M + i\omega C \tag{11}$$

By regimentation of the imaginary and real parts, the Novak's soil impedance K_u presented in Eq. (9), can be written as Eq. (12)

$$K_u = G_s\pi f(a_0,\nu_s,D) = G_s\pi\begin{Bmatrix}\mathrm{Re}[f(a_0,\nu_s,D)]\\ +i\,\mathrm{Im}[f(a_0,\nu_s,D)]\end{Bmatrix} \tag{12}$$

The Novak impedance (K_u) is estimated as a quadratic polynomial in a_0 by the Pacheco model (Pacheco *et al.* 2008). Therefore, K_u is identical to the dynamic impedance of an SDOF model (see Fig. 4(a) and Eq. (9)). By consideration of the imaginary and real components of the complex function $f(a_0,\nu_s,D)$, the expression of K_u can be written as follow

$$\mathrm{Re}[f(a_0,\nu_s,D)] \approx \alpha_k - \alpha_m a_0^{\,2}$$

$$\mathrm{Im}[f(a_0,\nu_s,D)] \approx \alpha_c a_0 \tag{13}$$

$$K_u \approx G_s\pi(\alpha_k - \alpha_m a_0^{\,2} + i\alpha_c a_0)$$

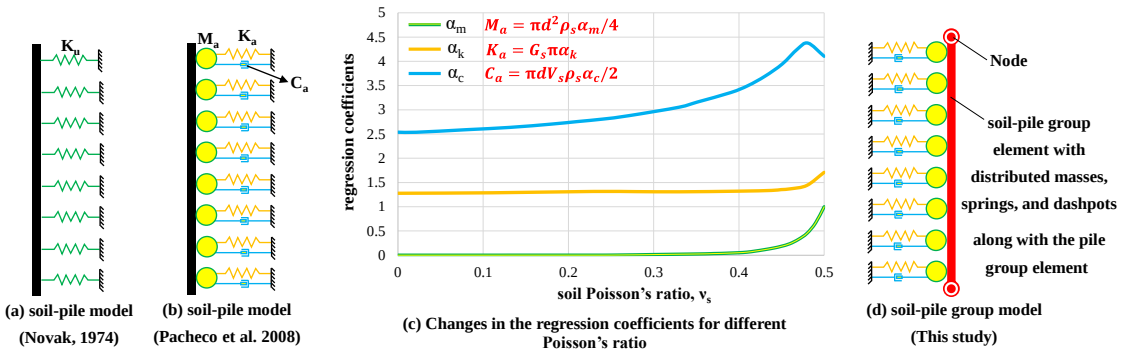

Fig. 4 Different dynamic models of soil-pile elements

By comparing the K_u parameter given by Eq. (13) with the impedance of an SDOF model in Eq. (11), it can be inferred that the stiffness factor K_a, the viscous dashpot factor C_a, and the lumped mass M_a are as Eq. (14)

$$K_u \approx K_a - M_a \omega^2 + iC_a \omega$$

$$M_a = \pi d^2 \rho_s \alpha_m / 4 \qquad (14)$$

$$K_a = G_s \pi \alpha_k$$

$$C_a = \pi d V_s \rho_s \alpha_c / 2$$

Note that the factors (K_a, M_a, and C_a) in the simple expressions of Eq. (14) provide an estimation of Novak's model, and these factors were considered per unit of pile length. The lumped mass model in the Pacheco study (Pacheco *et al.* 2008) is illustrated in Fig. 4(b). The coefficients of α_m, α_k, and α_c in Eq. (14) are obtained by the least-squares estimation of Novak's impedance functions according to Eq. (10). In this method, the soil-pile interaction can be considered through the springs with the stiffness K_a, the viscous dampers C_a, and the lumped masses M_a (Fig. 4(b)). All three mentioned factors are frequency independent. Also, the variations of the regression coefficients (α_m, α_k, and α_c) for wide ranges of soil Poisson's ratios from 0 to 0.5 are shown in Fig. 4(c).

The values of K_a, M_a, and C_a corresponding to the soil were determined by Pacheco in 2008 (Pacheco *et al.* 2008), but their applications (in bridges), the group performance of soil-pile elements, and the required dynamic analyses to detect the accuracy of the proposed model were neglected.

All of the values and equations in the Pacheco study (Pacheco *et al.* 2008) were presented by the consideration of the sole pile without any pile cap and pile group effects. By the proposed model of this study, the whole dynamic equations of a bridge are presented considering the capped pile group effects in the nonhomogeneous layered soil. Besides, Pacheco *et al.* (2008) has used lumped pile-soil model, but the present study focuses on the pile elements with distributed soil parameters. Unlike lumped models, the proposed distributed model does not need the discretization of piles into several finite elements. In the distributed models resolution of the system is provided by selecting the appropriate shape functions.

2.2.2 Formation of a soil-pile element using virtual work method

In this section, a series of consistent mass (M_a), stiffness (K_a), and damping (C_a) factors are obtained for a sole pile using a proper variational principle for pile elements together with the surrounding soils (as distributed parameters) and will be extended for the pile group in Section 2.3. This is done by adding together the stiffness of each pile in the pile group (due to their parallel performance) and by integrating a suitable efficiency coefficient (R) for the pile group with O piles (O is the number of piles in the pile group). The pile group element is shown in Fig. 4(d). It should be noted that the pile element with distributed soil parameters is considered and the masses, springs, and dashpots describing the soil medium are not lumped at the end points of the pile element. Consequently, the soil-pile model is composed of a pile (continuous beam element) with the surrounding soil (springs, dashpots, and masses). The generalized D'Alambert Principle (the Principle of Virtual Work), is given in Eq. (15) for a dynamic structural system (Clough and Penzien 1975)

$$\delta W_{\text{int}} - \delta W_{ext} - \delta W_{iner} = 0 \qquad (15)$$

Where δW_{int}, δW_{ext}, and δW_{iner} are the virtual works due to the internal forces, external forces, and inertial forces. For beam elements subject to the distributed forces $f(x,t)$ the three virtual work expressions are as Eq. (16)

$$\delta W_{ext} = \int_0^L f(x,t)\delta\eta(x,t)dx$$

$$\delta W_{\text{int}} = \int_0^L EI\eta''(x,t)\frac{d(\delta\eta(x,t))}{dx^2}dx \qquad (16)$$

$$\delta W_{iner} = -\int_0^L \overline{m}\,\ddot{\eta}(x,t)\delta\eta(x,t)dx$$

In which $\eta(x,t)$ denotes the transverse displacement, and $\delta\eta(x,t)$ denotes the virtual transverse displacement, $\overline{m} = \rho_{pile}A_{pile} + M_a$ denotes the distributed soil-pile mass per unit length. I and E denote the cross-section moment of inertia and the pile Young's modulus, respectively.

According to the finite element approach, the following expressions in Eq. (17) can be achieved

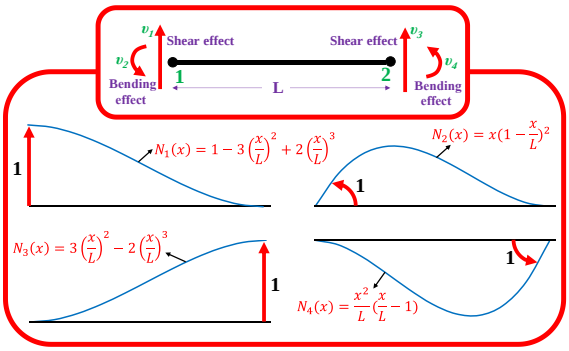

Fig. 5 Beam element shape functions

$$\eta(x,t) = [N(x)]\{\Phi(t)\}$$
$$\eta''(x,t) = [N''(x)]\{\Phi(t)\}$$
$$\delta\eta(x,t) = [N(x)]\{\delta\Phi(t)\} = \{\delta\Phi(t)\}^T[N(x)]^T \quad (17)$$
$$\delta\eta''(x,t) = [N''(x)]\{\delta\Phi(t)\} = \{\delta\Phi(t)\}^T[N''(x)]^T$$

In the above equation, *N(x)* and *Φ(t)*, respectively, denote the vector of the shape function and the displacement vector. To attain the stiffness, mass, and damping matrices, the Hermite shape function (Phoon and Huang 2012) is selected as Fig. 5 and Eq. (18).

$$[N] = [N_1 \quad N_2 \quad N_3 \quad N_4]^T$$
$$[\Phi] = [\eta_1 \quad \eta_2 \quad \eta_3 \quad \eta_4]^T \quad (18)$$

Therefore, the internal virtual work can be written as Eq. (19)

$$\delta W_{\text{int}} = \int_0^L EI\eta''(x,t)\delta\eta''(x,t)dx = \int_0^L EI\delta\eta''(x,t)\eta''(x,t)dx$$
$$\delta W_{\text{int}} = \{\delta\Phi(t)\}^T\left[\int_0^L EI[N''(x)]^T[N''(x)]dx\right]\{\Phi(t)\} \quad (19)$$

The stiffness matrix of the beam element $[k_b]$ can be defined as Eq. (20)

$$[k_b] = \left[\int_0^L EI[N''(x)]^T[N''(x)]dx\right] \quad (20)$$

The internal virtual work is simplified as Eq. (21)

$$\delta W_{\text{int}} = \{\delta\Phi(t)\}^T[k_b]\{\Phi(t)\} \quad (21)$$

If *f(x,t)* represents the distributed spring force and damper, $f(x,t) = -K_a\eta(x,t) - C_a\dot{\eta}(x,t)$, the virtual work due to the external force can be written as Eq. (22)

$$\delta W_{ext} = -\int_0^L K_a\eta(x,t)\delta\eta(x,t)dx - \int_0^L C_a\dot{\eta}(x,t)\delta\eta(x,t)dx \quad (22)$$

In the velocity field, by applying the finite element approach as Eq. (23)

$$\dot{\eta}(x,t) = [N(x)]\{\dot{\Phi}(t)\}$$
$$\delta\dot{\eta}(x,t) = [N(x)]\{\delta\dot{\Phi}(t)\} = \{\delta\dot{\Phi}(t)\}^T[N(x)]^T \quad (23)$$

The external virtual works can be rewritten as Eq. (24)

$$\delta W_{ext} = -\int_0^L K_a\delta\eta(x,t)\eta(x,t)dx - \int_0^L C_a\delta\eta(x,t)\dot{\eta}(x,t)dx$$
$$\rightarrow \delta W_{ext} = -\{\delta\Phi(t)\}^T\left[\int_0^L K_a[N(x)]^T[N(x)]dx\right]\{\Phi(t)\} \quad (24)$$
$$-\{\delta\Phi(t)\}^T\left[\int_0^L C_a[N(x)]^T[N(x)]dx\right]\{\dot{\Phi}(t)\}$$

By introducing the soil stiffness $[k_s]$ and damping $[c_s]$ matrices as Eq. (25)

$$[k_s] = \left[\int_0^L K_a[N(x)]^T[N(x)]dx\right]$$
$$[c_s] = \left[\int_0^L C_a[N(x)]^T[N(x)]dx\right] \quad (25)$$

The external virtual work is rewritten as Eq. (26)

$$\delta W_{ext} = -\{\delta\Phi(t)\}^T[k_s]\{\Phi(t)\} - \{\delta\Phi(t)\}^T[c_s]\{\dot{\Phi}(t)\} \quad (26)$$

Finally, with regards to the nodal coordinates, the acceleration field is expressed as Eq. (27)

$$\ddot{\eta}(x,t) = [N(x)]\{\ddot{\Phi}(t)\}$$
$$\delta\ddot{\eta}(x,t) = [N(x)]\{\delta\ddot{\Phi}(t)\} = \{\delta\ddot{\Phi}(t)\}^T[N(x)]^T \quad (27)$$

Substituting the acceleration expression into the relationship of the inertial virtual work leads to Eq. (28)

$$\delta W_{iner} = -\int_0^L \overline{m}\delta\eta(x,t)\ddot{\eta}(x,t)dx$$
$$\delta W_{iner} = -\{\delta\Phi(t)\}^T\left[\int_0^L \overline{m}[N(x)]^T[N(x)]dx\right]\{\ddot{\Phi}(t)\} \quad (28)$$

By defining the consistent mass matrix $[M_{\text{beam-soil}}]$ for the beam element (with the contribution of $[M_b]$) and considering the distributed mass of the soil (with the contribution of $[M_s]$) as Eq. (29)

$$[M_{beam-soil}] = \int_0^L \overline{m}[N(x)]^T[N(x)]dx =$$
$$\int_0^L (\rho_{pile}A_{pile} + m_a)[N(x)]^T[N(x)]dx$$
$$[M_{beam}] = \int_0^L (\rho_{pile}A_{pile})[N(x)]^T[N(x)]dx \quad (29)$$
$$[M_{soil}] = \int_0^L (m_a)[N(x)]^T[N(x)]dx$$

The virtual work expression for inertial forces is arranged as Eq. (30)

$$\delta W_{iner} = -\{\delta\Phi(t)\}^T[M_{beam-soil}]\{\ddot{\Phi}(t)\} \quad (30)$$

The principle of virtual works is concluded as follows in Eq. (31), using the above nomenclature

$$\delta W_{\text{int}} - \delta W_{ext} - \delta W_{iner} = 0 \rightarrow$$
$$\{\delta\Phi(t)\}^T\begin{bmatrix}[k_b]\{\Phi(t)\} + [k_s]\{\Phi(t)\} \\ +[c_s]\{\dot{\Phi}(t)\} + [M_{beam-soil}]\{\ddot{\Phi}(t)\}\end{bmatrix} = 0 \quad (31)$$

Forasmuch as the virtual displacement {δΦ} is generally arbitrary, the equations of motion for the soil-pile element can be obtained as Eq. (32)

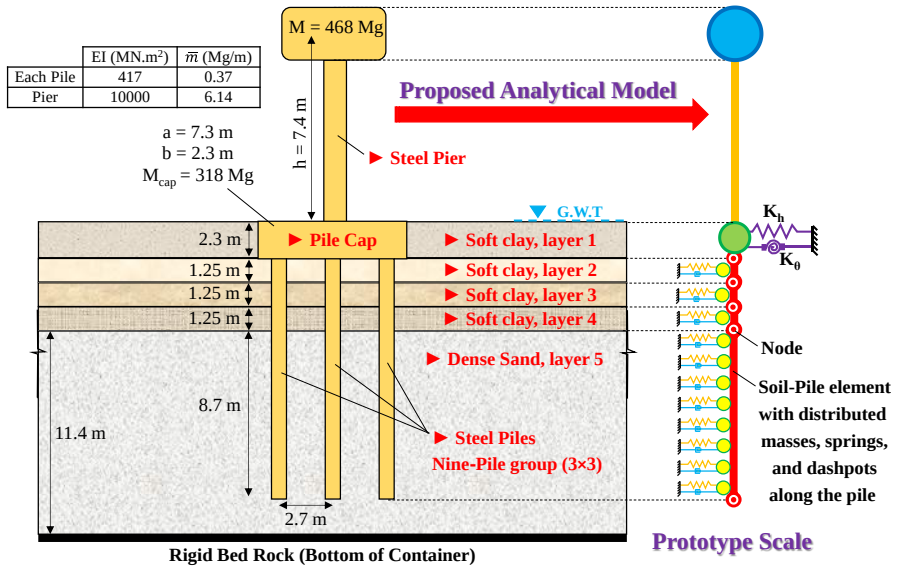

Fig. 6 The characteristics of centrifuge tests and the analytical model for validation

$$[k_b]\{\Phi(t)\}+[k_s]\{\Phi(t)\}+[c_s]\{\dot{\Phi}(t)\}+[M_{beam-soil}]\{\ddot{\Phi}(t)\}=0 \quad (32)$$

2.3 Assembling process and equation of motion

The global simplified model with seven DOFs, presented in Fig. 3, is considered for the case of an isolated bridge on one homogenous or nonhomogeneous soil layer and equipped with the pile group. The stiffness, mass, and damping matrices of this system are assembled using the superposition principle, as shown in Appendix A. A set of second-order linear differential equations is utilized to describe the equations of motion for a dynamic system as given by Eq. (33)

$$M\ddot{u}+C\dot{u}+Ku=-M\ddot{u}_g \quad (33)$$

This differential equation is solved numerically using Newmark's β method. The value of 0.25 is adopted for β to obtain stable and accurate solutions.

3. Validation of the proposed analytical model for homogenous soils

A number of seismic centrifuge tests of pile-supported structures conducted by Wilson (Wilson 1998) at the University of California-Davis were considered to validate the proposed analytical model. The model consists of a structure supported by nine piles (a 3×3 pile group), all placed in a profile of soft clay over a dense sand layer. Nine different excitations with a peak base acceleration of 0.016 g to 0.70 g (named Csp4-B, C, D, E, and Csp5-A, B, C, D, E) were applied to the base of the model. Fig. 6 illustrates the soil profile and the instrumentation for the tests. Details of the experimental data and results are available in Curras *et al.* (2001) and Wilson (1998). Two time history accelerations of Santa Cruz in 1989, Loma Prieta earthquake, with maximum accelerations of 0.035 g, 0.12 g, 0.3 g, 0.6 g, and of Port Island in 1995, Hyogoken-Nambu (Kobe) earthquake, with maximum accelerations of 0.016 g, 0.055 g, 0.2 g, 0.58 g, and 0.7 g were applied as excitations.

Table 1 Input parameters for the soil in the dynamic centrifuge tests (Rahmani *et al.* 2018)

Parameter	Layer 1	Layer 2	Layer 3	Layer 4	Layer 5
G_s (MPa)	0.5	1.3	1.8	2.4	41.5
ρ_s (kg/m^3)	1800	1830	1860	1890	2040
ν_s	0.49	0.49	0.49	0.49	0.48
α_m	0.682	0.682	0.682	0.682	0.457
α_k	1.611	1.611	1.611	1.611	1.463
α_c	4.389	4.389	4.389	4.389	4.338

All the components of the structure remained elastic under all earthquake events (Curras *et al.* 2001). It should be noted that the seismic behavior of the aforementioned structure can be considered as the seismic transversely behavior of a non-isolated bridge. The main goal of this validation is to check out the accuracy of an analytical model considering soil-pile-structure interaction in comparison to an inelastic experimental model in a lab. However, the verification will also be done in Section 4 for an isolated bridge on the inhomogeneous soil profile in a realistic condition. The specifications of soil layers are mentioned in Table 1 to be utilized in the proposed analytical model (Rahmani *et al.* 2018).

The NCHRP REPORT 461 (Program 2001) recommended that for the pile groups with the $S_p/d \geq 3$, group effects can be neglected (e.g., R = 1) during the lateral earthquake loading, where S_p is the center-to-center pile spacing in the pile group. Through the 1D free field analyses, the soil responses at various depths along the pile were estimated during each ground motion. The procedure is as follows: the bedrock time history acceleration is an

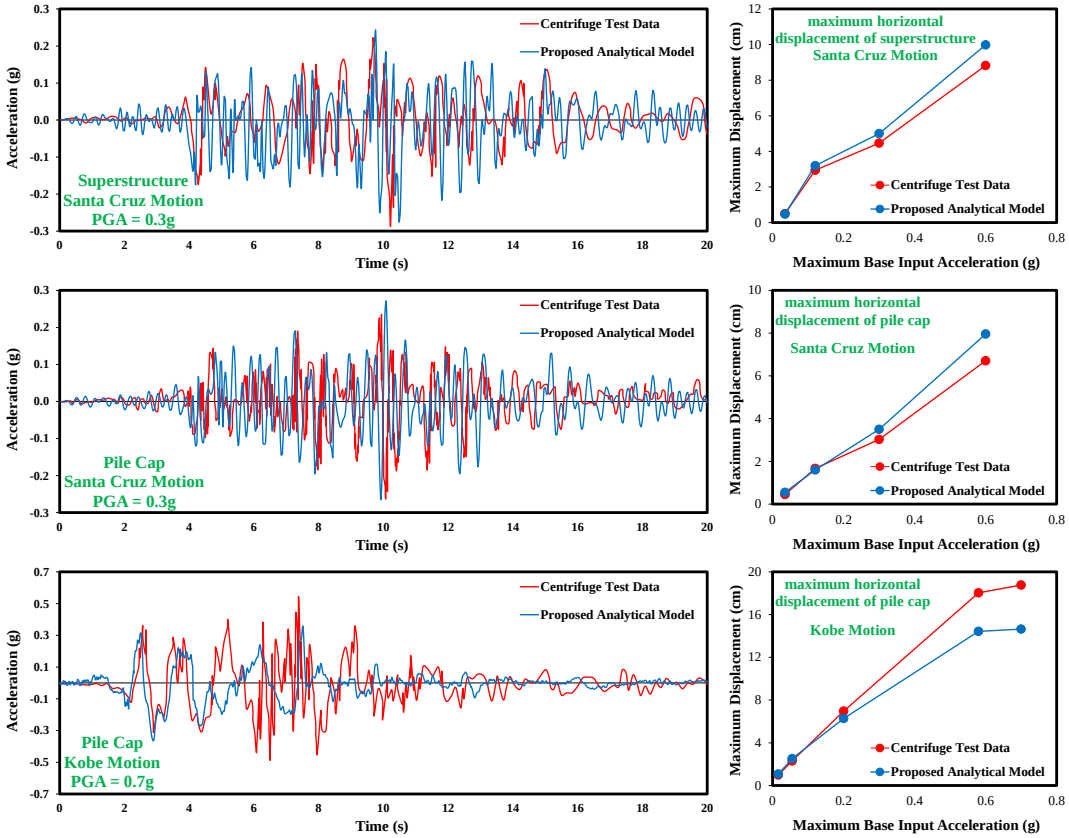

Fig. 7 Experimental and analytical responses with different maximum base input accelerations

input excitation at the bottom of the 1D soil column as an outcrop motion. Then, the motions at the depths along the pile are calculated separately as "within" motions and the obtained soil responses are applied to the ends of the soil springs. This procedure can simulate the effects of boundary conditions and is utilized in many previous studies (Kampitsis *et al.* 2013). Fig. 7 compares the responses of the computed and measured actions at the pile cap and the superstructure under the earthquakes with various maximum accelerations.

As shown, excellent conformity is seen between the results in different locations of the system, which validates the ability of the proposed model to consider SPSI for moderate (or low) excitations. Hence, the analytical model can provide reliable modeling of the SPSI problem. As depicted in Fig. 7, the results of the proposed model in the case of severe excitations are less than the values of the experimental model, and the precision of the proposed model is decreased by increasing base acceleration. This is due to the inelastic behavior of soil and the presence of soil permanent responses by increasing base accelerations. Also, in approximately the first three seconds of the earthquake record, the responses of the analytical model and the laboratory results are perfectly matched. The reason for this can be attributed to the lack of earthquake acceleration with strong amplitudes and the reduction of the effects of nonlinear soil behavior. The results for the other earthquake records are similar to Fig. 7 but are not shown here to avoid prolongation.

4. Verification of the proposed model for inhomogeneous soils

In nature, there is not any nonhomogeneous soil in which its specification can be exactly expressed by a mathematical function. In the laboratory, making a human-made soil profile in which its specification can be exactly expressed by a simple function is also too difficult. So, in this section, a numerical model is utilized to verify the proposed analytical model. It should be noted that the validation of the numerical model is provided in the author's previous papers (Shamsi *et al.* 2021).

4.1 Developed numerical model

In order to compare proposed analytical and numerical models, the Qom Monorail Bridge (QMB) is selected. This single-pier bridge is built with several sections which are disjoined by appropriate expansion joints to behave independently due to seismic loads. Herein, a stick model of a bridge section (with 4 spans of 17.5 meters, a total of 70 meters in length) without any horizontal and vertical curves is simulated by some rigid and elastic beam elements as shown in Fig. 8. Three target nodes are considered to evaluate responses, namely, A on the top of the bridge pier, B in the middle of the main beam, and C on the pile cap.

The height of the bridge pier is 12 meters, and the shear modulus of the isolator is 0.7 GPa with K_{xb} = 1890 kN/m and C_{xb} = 66.28 kN.s/m.

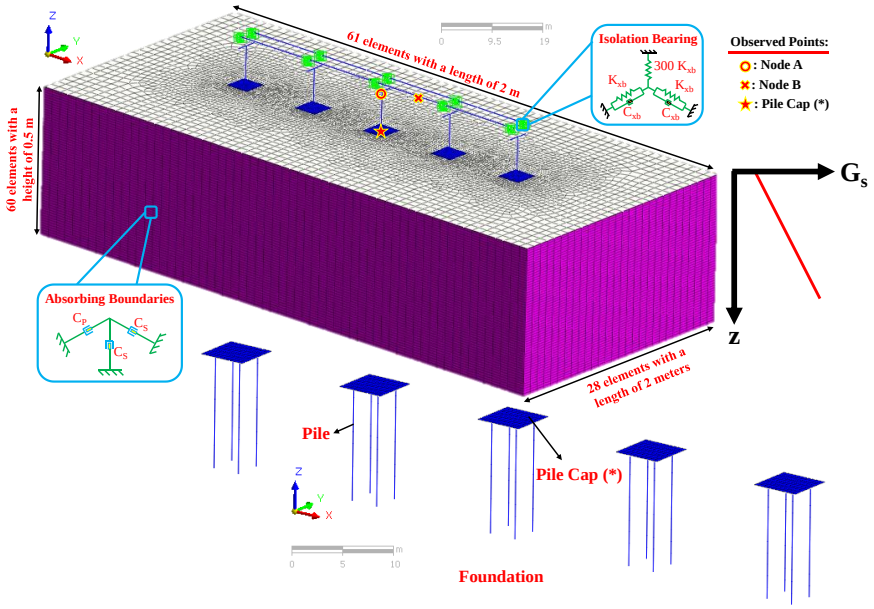

Fig. 8 Finite elements model of QMB under train load in the MIDAS GTS NX (2019)

To access modeling details such as configurations of the structural components, size of elements, element types, validation of the numerical model, boundary conditions, and site properties of the QMB used in the 3D continuum model refer to the other author's paper (Shamsi *et al*. 2021). Based on the geotechnical report, the QMB is supported by a four-pile group, which is founded in soil type C (180 m/s $<Vs_{,30}<$ 360 m/s), according to Eurocode 8. Poisson's ratio and the density of soil alluvium were assumed to be 0.3 (e.g., α_m, α_k, and α_c are 0, 1.23, and 2.49) and 1675 kg/m^3, respectively. In this study, it is assumed that the shear modulus (G_Z) of the site is changed along with the depth (z) as Eq. (34) as shown in Fig. 9 (a combination of uniform and proportional soil profiles). The average shear wave velocity at the top 30 m of soil profiles ($Vs_{,30}$= 336 m/s) was obtained by Eq. (35) based on Eurocode 8 (EN 2004); in which h_i and Vs_i denote the thickness (in meters) and the shear wave velocity of the i-th formation.

$$G(MPa) = S'z + P = 12z + 51 \tag{34}$$

$$Vs_{,30} = \frac{30}{\sum \frac{h_i}{Vs_i}} \tag{35}$$

Also, the specification of the QMB foundation is mentioned in Table 2. In this study, a series of seven earthquake excitations with different peak ground accelerations (PGAs) are scaled to the appropriate response spectrum. The criteria for records selection are based on the spectro-compatibility with the Eurocode 8 (EN 2004) design spectrum and correspond to the bedrock spectrum of ground type A (with a $Vs_{,30}>$ 800 m/s). The minimum durations of strong motions (D5-D95) are 10 seconds (EN 2004). Seismic records are applied transversely to the base of the numerical model. The specifications of the aforementioned records utilized for the verification are listed in Table 3.

Table 2 Characteristics of foundations of the QMB

Concrete bridge	QMB
Pile length (m)	12
Pile diameter (m)	1
The center-to-center spacing of piles (m)	3
Pile cap dimensions (m)	5×5×1.2

4.2 Developed analytical model

A series of consistent mass [M_{system}], stiffness [K_{system}], and damping [C_{system}] matrices are presented in Appendix A for a simplified analytical model with seven DOF and a unique soil-pile element. In the analytical model, to increase the precision, the pile is discretized into linear elastic beam elements with a length of 0.5 m (24 soil-pile elements) as shown in Fig. 9. The mass of the deck and isolation characteristics are modeled, while the distributed mass of the extended pile is simulated on the beam-element nodes.

The values of soil-pile-structure model parameters are presented in Tables 4 and 5. The mass matrix is calculated by Eqs. (A3-A4) and the stiffness of each soil-pile element is calculated by assembling stiffness for the case of the uniform soil profile and the proportional soil profile. By some references (Program 2001), neglecting group effects during the seismic loading is advised for the sandy soil, e.g., R =1. Fig. 10 presents a good agreement between the time history of the foundation response in the numerical and the analytical model. This type of agreement can be also seen for the three aforementioned observed points in Fig. 11 due to the seven seismic records. Fig. 11 depicts the absolute deviation percentage for approximating the maximum displacements of the QMB in the case of all input excitations. The error value is defined as the subtraction of the numerical model response (NMR) from the analytical model response (AMR) divided by the NRM and is appropriately calculated through Eq. (36).

Table 3 Characteristics of the selected earthquake records and their scale factors

#	Earthquake	Station	Year	$Vs_{,30}$ (m/s)	Strong motion duration (s)	PGA (g)	Scale Factor
1	Chi-Chi, Taiwan	CHY102	1999	804.36	18.6	0.064	1.85
2	Chuetsu-oki	FKSH07	2007	828.95	22.4	0.045	2.66
3	San Simeon, CA	Diablo Canyon Power Plant	2003	1100	16.9	0.047	2.55
4	Tottori, Japan	OKYH02	2000	1047.01	14.5	0.042	2.85
5	Whittier Narrows	Vasquez Rocks Park	1987	996.43	9.2	0.062	1.93
6	Iwate, Japan	MYG011	2008	1423.8	20.2	0.083	1.44
7	Loma Prieta	SF - Pacific Heights	1989	1249.86	11.9	0.062	1.93

Table 4 The parameters related to the pile cap in the analytical model

Parameter	k_h	k_θ	$k_{h\theta} = k_{\theta h}$	c_h	c_θ	$c_{h\theta} = c_{\theta h}$
Unit	MN/m	MN.m	MN	MN.s/m	MN.s.m	MN.s
Value	772.61	5152.29	152.56	6.72	16.56	4.01

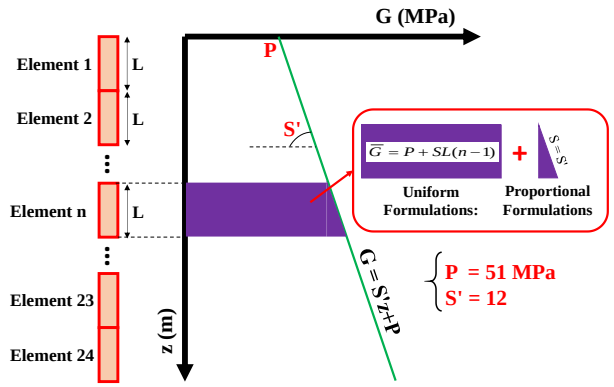

Fig. 9 Analytical simulation of piles and surrounding soil with 24 soil-pile elements

$$Error(\%)=\frac{\left\|AMR\right|-\left|NMR\right\|}{\left|NMR\right|}\times 100 \quad (36)$$

As can be seen, the error values in different nodes are less than 11% and the analytical model can be utilized to predict the Soil-Pile-Isolated Bridge seismic responses with acceptable accuracy.

5. Comparing the results of the proposed analytical model with other previous studies (modal analysis)

Eigenvalue analysis is one of the most basic analyses to investigate the behavior of structures in seismic conditions. By calculating the fundamental period and the vibration modes of a bridge, engineers can make the necessary corrections before the final design. In order to evaluate the performance of the analytical model for estimating the fundamental period of the system, modal analysis was performed. The accuracy of the model has been checked by comparing its results with the results obtained from the eigenvalue analysis of some isolated bridges by previous researchers. The soil profile was considered homogeneous and isotropic. The characteristics of the pile group, pile cap, and superstructure as well as the results of the comparisons are summarized in Table 6. The periods calculated by the analytical model are close to the values presented in other case studies. This shows that the equations can be used for other similar projects. One reason for matching the results is that the basic assumptions of the models are almost the same. However, the main reason for the difference between the results is related to the small distances between the piles and the effects of the efficiency coefficient for the pile group (R). Moreover, the asymmetric arrangements of the piles and the non-squareness of the pile caps are other factors for these differences. The relatively complex geometries of some bridge components (such as the bridge piers and pier heads) have also caused an increase in the percentage of errors in the calculation of free vibration periods of the bridges in the lateral direction. In some cases, the soil profile is assumed to be homogeneous and the average value of the soil shear modulus (G_s^{ave}) has been used to calculate the free vibration periods of the bridge-soil-pile system, which can lead to few errors.

Table 5 The parameters related to the main elements of the bridge

Parameter	M_d (for deck length of 17.5 m)	K_{xb}	C_{xb}	M_{ph}
Unit	Ton	kN/m	kN.s/m	Ton
Value	72.66	1890	66.28	40.32

6. Conclusions

In the present study, the soil-pile-structure interaction of isolated bridges is analyzed by a simplified model during moderate seismic loads. To investigate the effects of soil inhomogeneity along with the depth, the structural formulas in terms of closed-form solution were analytically presented for three different cases (a uniform (n=0), a proportional (n=1), and a parabolic (n=0.5) distribution of soil stiffness

Table 6 Comparison of modal analysis results obtained from the proposed analytical model and other past studies

Parameter	M_d	M_{ph}	I_{ph}	h	EI_{pier}	EI_{pile}	d	S_p/d	O_{pile}	L	G_s^{ave}	ν_s	a	a'	b	k_{xb}	**T^***	**$T^\$$**	**Δ**
Bridge [Study] / Unit	Ton	Ton	ton.m^2	m	GN.m^2	GN.m^2	m	---	#	m	MPa	---	m	m	m	kN/m	**sec**	**sec**	**%**
Bridge I (Ucak and Tsopelas 2008)	265	38.5	---	5.2	4.84	0.031	0.43	2.5	25	21.5	22	0.4	5.16	5.16	1.1	2615.4	**2.14**	**2.49**	**16.36**
A14 motorway overcrossing (Dezi *et al.* 2012)	203.6	---	---	10	819.2	2.443	1.2	3	8	20	148.6	0.47	12.8	5.6	1.5	2010	**2.2**	**2.39**	**8.64**
Bridge II (Papathanasiou *et al.* 2016)	1440	620	---	40	1939.6	9.523	1.8	2.5	25	21.5	22	0.4	21.6	21.6	3	2807.3	**4.85**	**4.51**	**-7.01**
A typical bridge (Tubaldi *et al.* 2018)	760.5	54	122.62	10	57.52	0.603	0.8	3	9	18	174.1	0.4	6	6	2.5	7506.2	**2.04**	**2.29**	**12.09**
QMB-I (Shamsi and Ghanbari 2020)	72.66	44.2	92.59	13	7.08	1.080	1	3	4	12	122.1	0.3	5	5	1.2	1890	**1.17**	**1.26**	**7.69**
Taiwan railway bridge (Shamsi *et al.* 2021)	278.9	130	335.73	12	111.78	17.279	2	7.8	4	24	122.1	0.3	10.8	10.8	2.8	3457.2	**1.75**	**1.66**	**-5.14**

T^*: The vibration period of the isolated bridge considering SSI reported in previous studies; $T^\$$: The vibration period of the isolated bridge considering SSI from the proposed analytical model; Δ: The relative difference between the results of the proposed model and the data from the previous studies; Pile cap dimensions: a×a'×b

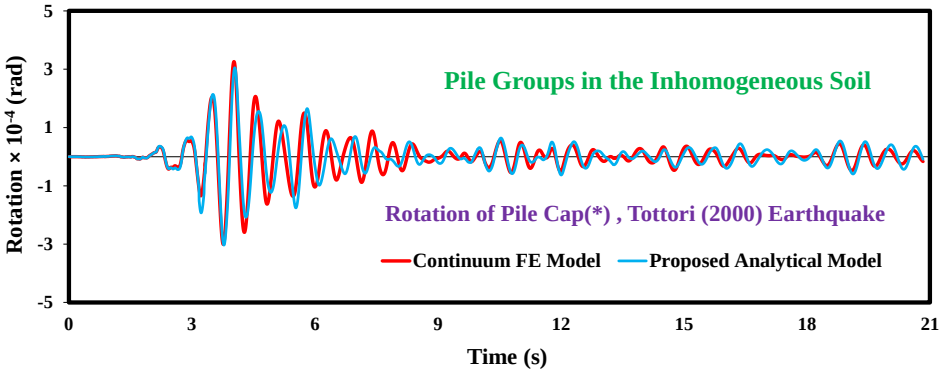

Fig. 10 Linearly dynamic responses (rotation of piles cap) in the proposed analytical and numerical modeling under the Tottori earthquake (2000)

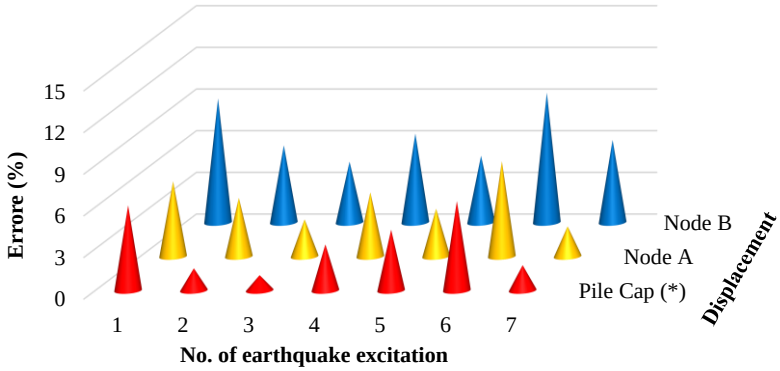

Fig. 11 Absolute percentage errors in maximum displacement responses at various observed points of the numerical model

with depth). Also, to validate the analytical model performance in predicting the seismic behavior of the soil-pile-bridge system, modal and dynamic analyses were conducted. The primary findings derived from this investigation are as follows:

- The presented analytical model can predict the seismic behavior of alluvium in which the shear modulus is non-constant in the depth. This model can simulate the behavior of structures located on the pile considering

the inhomogeneity effect of soil shear modulus along the depth.

- As a result of its analytical approach, less effort and time are needed in the analysis process in comparison to the numerical procedure. Therefore, this simple analytical model of a beam on the elastic foundation can be added to numerical commercial software.
- The proposed distributed soil model does not need discretization of piles into several finite elements and resolution of the system is provided by selecting the appropriate shape functions. Thus, by reducing the DOF of the system, the proposed model may obtain accurate responses with minimum computational time.
- As reviewed, the quantities of deviation in estimated responses are less than 11% compared with the numerical results; therefore, the proposed model can be utilized to predict the Soil-Pile-Isolated Bridge responses for moderate earthquakes with acceptable accuracy.
- The deviation of estimated responses in the case of severe earthquakes is considerable. This originates in the fact that the linear viscoelastic behavior hypothesis has been applied to represent the pile and soil kinematic behaviors; and accordingly, stiffness degradation effects are not considered by strain-compatible moduli in the process.
- In modal analysis, the main reason for matching the results is that the basic assumptions of different models are almost the same. Among the main reasons for the difference between the results can be attributed to the asymmetric arrangement of the piles, the non-squareness of the pile caps in some studies, the small distances between the piles, and the significant effects of the efficiency coefficient of the pile group.

The relatively complex geometries of some bridge components, such as the bridge pier and pier heads, have also caused an increase in the percentage of errors in the calculation of free vibration periods of isolated bridges in the lateral direction. In some cases, the soil profile is assumed to be homogeneous by considering the simplifying assumptions and the average value of the shear modulus of the soil has been used to calculate the periods of the bridge-soil-pile system, which can lead to few errors.

Acknowledgments

The authors would like to thank the University of Hormozgan, and the University of Garmsar for their partial support allocated to this research study.

References

AASHTO (1997), "Guide specifications for seismic isolation design, American association of state highway and transportation officials, Washington", *American Association of State Highway and Transportation Officials*, Washington, D.C., 2014, July.

Amornfa, K., Quang, H.T. and Tuan, T.V. (2023), "Effect of groundwater level change on piled raft foundation in Ho Chi Minh City, Viet Nam using 3D-FEM", *Geomech. Eng.*, **32**(4), 387-396. https://doi.org/10.12989/gae.2023.32.4.387.

Antoniadis, I.A., Kapasakalis, K.A. and Sapountzakis. E.J. (2019), "Isolation or Damping? A soil-dependent approach based on the KDamper concept", *Proceedings of the 2nd Int. Conf. Nat. Hazards Infrastruct.(ICONHIC 2019)*.

Carbonari, S., Morici, M., Dezi, F., Gara, F. and Leoni, G. (2017), "Soil-structure interaction effects in single bridge piers founded on inclined pile groups", *Soil Dyn. Earthq. Eng.*, **92**, 52-67. https://doi.org/10.1016/j.soildyn.2016.10.005.

Clough, R.W. and Penzien, J. (1975), *Dynamics of Structures*. McGraw-Hill.

Curras, C.J., Boulanger, R.W., Kutter, B.L. and Wilson, D.W. (2001), "Dynamic experiments and analyses of a pile-group-supported structure", *J. Geotech. Geoenviron. Eng.*, **127**(7), 585-596. https://doi.org/10.1061/(ASCE)1090-0241(2001)127:7(585).

Dezi, F., Carbonari, S., Tombari, A. and Leoni, G. (2012), "Soil-structure interaction in the seismic response of an isolated three span motorway overcrossing founded on piles", *Soil Dynam. Earthq. Eng.*, **41**, 151-163. https://doi.org/10.1016/j.soildyn.2012.05.016.

Di Laora, R., Mylonakis, G. and Mandolini, A. (2013), "Pile-head kinematic bending in layered soil", *Earthq. Eng. Struct. D.*, **42**(3), 319-337. https://doi.org/10.1002/eqe.2201.

Di Laora, R, and Rovithis, E. (2015), "Kinematic bending of fixed-head piles in nonhomogeneous soil", *J. Geotech. Geoenviron. Eng.*, **141**(4), 04014126. https://doi.org/10.1061/(ASCE)GT.1943-5606.0001270.

Elchiti, I., Saad, G. and Najjar, S.S. (2023), "Passive P-y curves for rigid basement walls supporting granular soils", *Geomech. Eng.*, **32**(3), 335-346. https://doi.org/10.12989/gae.2023.32.3.335.

Elgamal, A., Yan, L., Yang, Z. and Conte, J.P. (2008), "Three-dimensional seismic response of Humboldt Bay Bridge-foundation-ground system", *J. Struct. Eng.*, **134**(7), 1165-1176. https://doi.org/10.1061/(ASCE)0733-9445(2008)134:7(1165).

EN, BS. (2004), "Eurocode 8: Design of structures for earthquake resistance-part 5: Foundations, retaining structures and geotechnical aspects".

Gazetas, G. (1991), "Foundation vibrations", *Foundation engineering handbook*, Springer.

Gibson, R.E. (1974), "The analytical method in soil mechanics", *Geotechnique*, **24**(2), 115-140.

González, F., Carbonari, S., Padrón, L.A., Morici, M., Aznárez, J.J., Dezi, F., Maeso, O. and Leoni. G. (2020), "Benefits of inclined pile foundations in earthquake resistant design of bridges", *Eng. Struct.*, **203**, 109873. https://doi.org/10.1016/j.engstruct.2019.109873.

González, F., Padrón, L.A., Carbonari, S., Morici, M., Aznárez, J.J., Dezi, F. and Leoni, G. (2019), "Seismic response of bridge piers on pile groups for different soil damping models and lumped parameter representations of the foundation", *Earthq. Eng. Struct. D.*, **48**(3), 306-327.

Haouari, H. and Bouafia, A. (2023), "Single piles under cyclic lateral loads - full scale tests and numerical modelling", *Geomech. Eng.*, **32**(1), 21-34. https://doi.org/10.12989/gae.2023.32.1.021.

Jalili, J., Askari, F., Haghshenas, E. and Marghaiezadeh, A. (2023), "Investigation on economical method of foundation construction on soft soils in seismic zones: A case study in Southern Iran", *Geomech. Eng.*, **32**(2), 209-232. https://doi.org/10.12989/gae.2023.32.2.209.

Ju, S.H. (2013), "Improvement of bridge structures to increase the safety of moving trains during earthquakes", *Eng. Struct.*, **56**, 501-508. https://doi.org/10.1016/j.engstruct.2013.05.035.

Kampitsis, A.E., Sapountzakis, E.J., Giannakos, S.K. and

Gerolymos, N.A. (2013), "Seismic soil-pile-structure kinematic and inertial interaction-a new beam approach", *Soil Dyn. Earthq. Eng.*, **55**, 211-224. https://doi.org/10.1016/j.soildyn.2013.09.023.

Kapasakalis, K.A., Sapountzakis, E.J. and Antoniadis, I.A. (2018), "Kdamper concept in seismic isolation of building structures with soil structure interaction", *Proceedings of the 13th international conference on computational structures technology (CST2018)*.

Kapasakalis, K.A., Alvertos, A.E., Mantakas, A.G., Antoniadis, I.A. and Sapountzakis, E.J. (2020), "Advanced negative stiffness vibration absorber coupled with soil-structure interaction for seismic protection of buildings", *Proceedings of the Int Conf Struct Dyn EURODYN*. Vol. 2.

Kapasakalis, K.A., Antoniadis, I.A. and Sapountzakis, E.J. (2021), "A soil-dependent approach for the design of novel negative stiffness seismic protection devices", *Appl. Sci.*, **11**(14), 6295. https://doi.org/10.3390/app11146295.

Kapasakalis, K., Sapountzakis, E. and Antoniadis, I. (2018), "Optimal design of the kdamper concept for structres on compliant supports".

Karatzia, X. and Mylonakis, G. (2012), "Horizontal response of piles in inhomogeneous soil: Simple analysis", *Proceedings of the 2nd International Conference on Performance-Based Design in Earthquake Geotechnical Engineering*, Taormina, Italy. Paper.

Kunde, M.C. and Jangid, R.S. (2006), "Effects of pier and deck flexibility on the seismic response of isolated bridges", *J. Bridge Eng.*, **11**(1), 109-121. https://doi.org/10.1061/(ASCE)1084-0702(2006)11:1(109).

Lesgidis, N., Sextos, A. and Kwon, O.S. (2018), "A frequency-dependent and intensity-dependent macroelement for reduced order seismic analysis of soil-structure interacting systems", *Earthq. Eng Struct. D.*, **47**(11), 2172-2194. https://doi.org/10.1002/eqe.3063.

Limkatanyu, S., Sae-Long, W., Damrongwiriyanupap, N., Sukontasukkul, P., Imjai, T., Chompoorat, T. and Hansapinyo, C. (2023), "Nonlinear shear-flexure-interaction RC frame element on winkler-pasternak foundation", *Geomech. Eng.*, **32**(1), 69-84. https://doi.org/10.12989/gae.2023.32.1.069.

Mantakas, A.G., Kapasakalis, K.A., Alvertos, A.E., Antoniadis, I.A. and Sapountzakis, E.J. (2022), "A negative stiffness dynamic base absorber for seismic retrofitting of residential buildings", *Struct. Control Health Monit.*, **29**(12), e3127. https://doi.org/10.1002/stc.3127.

Mantakas, A., Tsatsis, A., Loli, M., Kourkoulis, R. and Gazetas, G. (2023), "Seismic response of a motorway bridge founded in an active landslide: A case study", *Bull. Earthq. Eng.*, **21**(1), 605-32. https://doi.org/10.1007/s10518-022-01544-3.

Maravas, A., Mylonakis, G. and Karabalis, D.L. (2014), "Simplified discrete systems for dynamic analysis of structures on footings and piles", *Soil Dyn. Earthq. Eng.*, **61-62**, 29-39. https://doi.org/10.1016/j.soildyn.2014.01.016.

Massumi, A. and Moshtagh, E. (2013), "A new damage index for RC buildings based on variations of nonlinear fundamental period", **22**(1), 50-61. https://doi.org/10.1002/tal.656.

Matsagar, V.A. and Jangid, R.S. (2008), "Base isolation for seismic retrofitting of structures", *Practice Periodical on Structural Design and Construction*, **13**(4), 175-185. https://doi.org/10.1061/(ASCE)1084-0680(2008)13:4(175).

Medina, C., Álamo, G.M., Padrón, L.A., Aznárez, J.J. and Maeso, O. (2019), "Application of regression models for the estimation of the flexible-base period of pile-supported structures in continuously inhomogeneous soils", *Eng. Struct.*, **190**, 76-89. https://doi.org/10.1016/j.engstruct.2019.03.112.

Moshtagh, E., Eskandari-Ghadi, M. and Pan, E. (2019), "Time-harmonic dislocations in a multilayered transversely isotropic magneto-electro-elastic half-space", **30**(13), 1-19. https://doi.org/10.1177/1045389X19849286.

Moshtagh, E., Pan, E. and Eskandari-Ghadi, M. (2017), "Wave propagation in a multilayered magneto-electro-elastic half-space induced by external/Internal circular time-harmonic mechanical loading", **128**, 243-261. http://dx.doi.org/10.1016/j.ijsolstr.2017.08.032.

Moshtagh, E., Pan, E. and Eskandari-Ghadi, M. (2018), "Shear excitation of a multilayered magneto-electro-elastic half-space considering a vast frequency content", **123**, 214-235. https://doi.org/10.1016/j.ijengsci.2017.11.012.

Mylonakis, G. and Gazetas, G. (2000), "Seismic soil-structure interaction: Beneficial or Detrimental?", *J. Earthq. Eng.*, 4(3), 277-301. https://doi.org/10.1080/13632460009350372.

Nikolaou, S., Mylonakis, G. Gazetas, G. and Tazoh, T. (2001), "Kinematic pile bending during earthquakes: Analysis and field measurements", *Géotechnique*, **51**(5), 425-440. https://doi.org/10.1680/geot.2001.51.5.425.

Novak, M. (1974), "Dynamic stiffness and damping of piles", *Can. Geotech. J.*, **11**(4), 574-598. https://doi.org/10.1139/t74-059.

Novak, M. and Aboul-Ella, F. (1978), "Impedance functions of piles in layered media", *J. Eng. Mech.Div.*, **104**(3), 643-661. https://doi.org/10.1061/JMCEA3.0002366.

Pacheco, G., Suárez, L.E. and Pando, M. (2008), "Dynamic lateral response of single piles considering soil inertia contributions", *Proceedings of the World Conference on Earthquake Engineering*, Beijing, China.

Papathanasiou, S.M., Tsopelas, P., Prapa, E. and Ucak, A. (2016), "Infulence of soil-structure interaction modeling on the response of seismically isolated bridges", *Int. J. Bridge Eng.*, 39-70.

Phoon, K.K. and Huang, S.P. (2012), "Uncertainty quantification using multi-dimensional hermite polynomials", 1-10. https://doi.org/10.1061/40914(233)12.

Program, National Cooperative Highway Research (2001), *Static and Dynamic Lateral Loading of Pile Groups*.

Qiu, Z., Ebeido, A., Almutairi, A., Lu, J., Elgamal, A., Shing, P.B. and Martin, G. (2020), "Aspects of bridge-ground seismic response and liquefaction-induced deformations", *Earthq. Eng. Struct. D.*, **49**(4), 375-393. https://doi.org/10.1002/eqe.3244.

Rahmani, A., Taiebat, M., Liam Finn, W.D. and Ventura, C.E. (2018), "Evaluation of P-y springs for nonlinear static and seismic soil-pile interaction analysis under lateral loading", *Soil Dyn. Earthq. Eng.*, **115**, 438-447. https://doi.org/10.1016/j.soildyn.2018.07.049.

Rahmani, A., Taiebat, M., Liam Finn, W.D. and Ventura, C.E. (2016), "Evaluation of substructuring method for seismic soil-structure interaction analysis of bridges", *Soil Dyn. Earthq. Eng.*, **90**, 112-127. https://doi.org/10.1016/j.soildyn.2016.08.013.

Rovithis, E.N., Pitilakis, K.D. and Mylonakis, G.E. (2011), "A note on a pseudo-natural SSI frequency for coupled soil–pile–structure systems", *Soil Dyn. Earthq. Eng.*, **31**(7), 873-878. https://doi.org/10.1016/j.soildyn.2011.01.006.

Saitoh, M. (2012), "On the performance of lumped parameter models with gyro-mass elements for the impedance function of a pile-group supporting a single-degree-of-freedom system", *Earthq. Eng. Struct. D.*, **41**(4), 623-641. https://doi.org/10.1002/eqe.1147.

Santisi d'Avila, M.P. and Lopez-Caballero, F. (2018), "Analysis of nonlinear soil-structure interaction effects: 3D frame structure and 1-directional propagation of a 3-component seismic wave", *Comput. Struct.*, **207**, 83-94. https://doi.org/10.1016/j.compstruc.2018.02.002.

Shabani, M.J, Shamsi, M. and Ghanbari, A. (2021a), "Dynamic response of three-dimensional mid-rise buildings adjacent to

slope under seismic excitation in the direction perpendicular to the slope", *Int. J. Geomech*., **21**(11), https://doi.org/10.1061/(ASCE)GM.1943-5622.0002158.

Shabani, M.J., Shamsi, M. and Ghanbari, A. (2021b), "Seismic response of RC moment frame including topography-soil-structure interaction", *Practice Periodical on Structural Design and Construction*, 26(4), https://doi.org/10.1061/(ASCE)SC.1943-5576.0000625.

Shabani, M.J., Shamsi, M. and Ghanbari, A. (2021), "Slope topography effect on the seismic response of mid-rise buildings considering topography-soil-structure interaction", *Earthq. Struct*., **20**(2), 187-200. https://doi.org/10.12989/eas.2021.20.2.187.

Shamsi, M., Zakerinejad, M. and Vakili, A.H. (2021), "Seismic analysis of soil-pile-bridge-train interaction for isolated monorail and railway bridges under coupled lateral-vertical ground motions", *Eng. Struct*., **248**, https://doi.org/10.1016/j.engstruct.2021.113258.

Shamsi, M. and Ghanbari, A. (2020), "Seismic retrofit of Monorail bridges considering soil–pile–bridge–train interaction", *J. Bridge Eng*., **25**(10), 04020075. https://doi.org/10.1061/(ASCE)BE.1943-5592.00016.

Shamsi, M., Shabani, M.J. and Vakili, A.H. (2022), "Three-dimensional seismic nonlinear analysis of topography–structure–soil–structure interaction for buildings near slopes", *Int. J. Geomech.*, **22**(3), 04021295. https://doi.org/10.1061/(ASCE)GM.1943-5622.000230.

Shamsi, M., Shabani, M.J.., Zakerinejad, M. and Vakili, A.H. (2022), "Slope topographic effects on the nonlinear seismic behavior of groups of similar buildings", *Earthq. Eng. Struct. D.*, **51**(10), 2292-2314. https://doi.org/10.1002/eqe.3664.

Spyrakos, C.C. (1992), "Seismic behavior of bridge piers including soil-structure interaction", *Comput. Struct*., **43**(2), 373-384. https://doi.org/10.1016/0045-7949(92)90155-S.

Spyrakos, C.C. (1990), "Assessment of SSI on the longitudinal seismic response short span bridges", *Constr. Build. Mater.*, **4**(4), 170-175. https://doi.org/10.1016/0950-0618(90)90036-Z.

Tongaonkar, N.P. and Jangid, R.S. (2003), "Seismic response of isolated bridges with soil-structure interaction", *Soil Dyn. Earthq. Eng.*, **23**(4), 287-302. https://doi.org/10.1016/S0267-7261(03)00020-4.

Tubaldi, E., Mitoulis, S.A. and Ahmadi, H. (2018), "Comparison of different models for high damping rubber bearings in seismically isolated bridges", *Soil Dyn. Earthq. Eng.*, **104**, 329-345. https://doi.org/10.1016/j.soildyn.2017.09.017.

Ucak, A. and Tsopelas, P. (2008), "Effect of soil–Structure Interaction on Seismic Isolated Bridges", *J. Struct. Eng*., **134**(7), 1154-1164. https://doi.org/10.1061/(ASCE)0733-9445(2008)134:7(1154).

Wilson, D.W. (1998), "Soil-pile-superstructure interaction in liquefying sand and soft clay", *Doctoral Dissertation, University of California, Davis*.

Wolf, J.P. (1985), *Dynamic Soil-Structure Interaction*, Englewood Cliffs, N.J: Prentice-Hall.

Xiong, W., Jiang, L.Z. and Li, Y.Z. (2016), "Influence of soil–structure interaction (Structure-to-soil relative stiffness and mass ratio) on the fundamental period of buildings: Experimental observation and analytical verification", *Bull. Earthq. Eng*., **14**(1), 139-160. https://doi.org/10.1007/s10518-015-9814-2.

Appendix A

The stiffness matrix of the system (Fig. 3) is

$$K_{system}=\begin{bmatrix} k_{11} & k_{12} & k_{13} & k_{14} & k_{15} & k_{16} & k_{17} \\ & k_{22} & k_{23} & k_{24} & k_{25} & k_{26} & k_{27} \\ & & k_{33} & k_{34} & k_{35} & k_{36} & k_{37} \\ & & & k_{44} & k_{45} & k_{46} & k_{47} \\ & & & & k_{55} & k_{56} & k_{57} \\ & sym. & & & & k_{66} & k_{67} \\ & & & & & & k_{77} \end{bmatrix}$$

$k_{11}=k_{xb}$; $k_{12}=-k_{xb}$; $k_{13}=k_{14}=k_{15}=k_{16}=k_{17}=0$

; $k_{22}=\dfrac{12EI_{Pier}}{h^3}+k_{xb}$; $k_{23}=k_{25}=\dfrac{6EI_{Pier}}{h^2}$;

$k_{24}=-\dfrac{12EI_{Pier}}{h^3}$; $k_{26}=k_{27}=0$; $k_{33}=\dfrac{4EI_{Pier}}{h}$;

$k_{34}=-\dfrac{6EI_{Pier}}{h^2}$; $k_{35}=\dfrac{12EI_{Pier}}{h}$; $k_{36}=k_{37}=0$;

$$k_{44}=\frac{12EI_{Pier}}{h^3}+\frac{8G_{sb/2}r_1}{2-\nu_s}\ ;\quad +O\times R\times\left(\frac{12EI_{Pile}}{L^3}+A_{11}\right)$$

$$k_{45}=-\frac{6EI_{Pier}}{h^2}+\frac{0.56G_{sb/2}r_1^{\,2}}{2-\nu_s}\ ;\quad +O\times R\times\left(\frac{6EI_{Pile}}{L^2}+A_{12}\right) \qquad \text{(A1)}$$

$k_{46}=O\times R\times\left(-\dfrac{12EI_{Pile}}{L^3}+A_{13}\right)$;

$k_{47}=O\times R\times\left(\dfrac{6EI_{Pile}}{L^2}+A_{14}\right)$;

$$k_{55}=\frac{4EI_{Pier}}{h}+\frac{8G_{sb/2}r_2^{\,3}}{3(1-\nu_s)}+O\times R\times\left(\frac{4EI_{Pile}}{L}+A_{22}\right)$$

; $k_{56}=O\times R\times\left(\dfrac{-6EI_{Pile}}{L^2}+A_{23}\right)$;

$k_{57}=O\times R\times\left(\dfrac{12EI_{Pile}}{L}+A_{24}\right)$;

$k_{66}=O\times R\times\left(\dfrac{12EI_{Pile}}{L^3}+A_{33}\right)$;

$k_{67}=O\times R\times\left(-\dfrac{6EI_{Pile}}{L^2}+A_{34}\right)$;

$k_{77}=O\times R\times\left(\dfrac{4EI_{Pile}}{L}+A_{44}\right)$

where

For the uniform case (n=0):

$$A=\pi\alpha_k\overline{G}\begin{bmatrix} \frac{13L}{35} & \frac{11L^2}{210} & \frac{9L}{70} & \frac{-13L^2}{420} \\ & \frac{L^3}{105} & \frac{13L^2}{420} & \frac{-L^3}{140} \\ & & \frac{13L}{35} & \frac{-11L^2}{210} \\ sym. & & & \frac{L^3}{105} \end{bmatrix}$$

For the proportional case (n=1):

$$A=\pi\alpha_k S\begin{bmatrix} \frac{3L^2}{35} & \frac{L^3}{60} & \frac{9L^2}{140} & \frac{-L^3}{70} \\ & \frac{L^4}{280} & \frac{L^3}{60} & \frac{-L^4}{280} \\ & & \frac{2L^2}{7} & \frac{-L^3}{28} \\ sym. & & & \frac{L^4}{168} \end{bmatrix} \qquad \text{(A2)}$$

For the parabolic case (n=0.5):

$$A=\pi\alpha_k G_{sd}\begin{bmatrix} a_{11} & a_{12} & a_{13} & a_{14} \\ & a_{22} & a_{23} & a_{24} \\ & & a33 & a_{34} \\ sym. & & & a_{35} \end{bmatrix}$$

$a_{11}=\dfrac{7424L^{1.5}}{45045d^{0.5}}$; $a_{12}=\dfrac{256L^{2.5}}{9009d^{0.5}}$;

$a_{13}=\dfrac{4016L^{1.5}}{45045d^{0.5}}$; $a_{14}=\dfrac{-928L^{2.5}}{45045d^{0.5}}$;

$a_{22}=\dfrac{256L^{3.5}}{45045d^{0.5}}$; $a_{23}=\dfrac{16L^{2.5}}{715d^{0.5}}$;

$a_{24}=\dfrac{-32L^{3.5}}{6435d^{0.5}}$; $a_{33}=\dfrac{694L^{1.5}}{2145d^{0.5}}$;

$a_{34}=\dfrac{-92L^{2.5}}{2145d^{0.5}}$; $a_{44}=\dfrac{16L^{3.5}}{2145d^{0.5}}$;

The mass matrix of the system (Fig. 3) is:

$$M_{system}=\begin{bmatrix} m_{11} & m_{12} & m_{13} & m_{14} & m_{15} & m_{16} & m_{17} \\ & m_{22} & m_{23} & m_{24} & m_{25} & m_{26} & m_{27} \\ & & m_{33} & m_{34} & m_{35} & m_{36} & m_{37} \\ & & & m_{44} & m_{45} & m_{46} & m_{47} \\ & & & & m_{55} & m_{56} & m_{57} \\ & sym. & & & & m_{66} & m_{67} \\ & & & & & & m_{77} \end{bmatrix}$$

$m_{11}=M_d$; $m_{13}=m_{14}=m_{15}=m_{16}=m_{17}=0$; (A3)

$m_{22}=M_{ph}+\dfrac{13}{35}\overline{m}_{Pier}h$; $m_{23}=\dfrac{11}{210}\overline{m}_{Pier}h^2$;

$m_{24}=\dfrac{9}{70}\overline{m}_{Pier}h$; $m_{25}=-\dfrac{13}{420}\overline{m}_{Pier}h$; $m_{26}=m_{27}=0$;

$m_{33}=I_{ph}+\dfrac{1}{105}\overline{m}_{pier}h^3$; $m_{34}=\dfrac{13}{420}\overline{m}_{Pier}h^2$;

$m_{35}=-\dfrac{1}{140}\overline{m}_{Pier}h^3$; $m_{36}=m_{37}=0$;

$$m_{44}=\frac{13}{35}\overline{m}_{pier}h+M_{cap}+O\times R\times(\frac{13}{35}\overline{m}_{pile}L+B_{11});$$

$$m_{45}=-\frac{11}{210}\overline{m}_{pier}h^2+O\times R\times(\frac{11}{210}\overline{m}_{pile}L^2+B_{12});$$

$$m_{46}=O\times R\times(\frac{9}{70}\overline{m}_{pile}L+B_{13});$$

$$m_{47}=O\times R\times(\frac{-13}{420}\overline{m}_{pile}L^2+B_{14});$$

$$m_{55}=\frac{1}{105}\overline{m}_{pier}h^3+I_{cap}+O\times R\times(\frac{1}{105}\overline{m}_{pile}L^3+B_{22});$$

$$m_{56}=O\times R\times(\frac{13}{420}\overline{m}_{pile}L^2+B_{23});$$

$$m_{57}=O\times R\times(\frac{-1}{140}\overline{m}_{pile}L^3+B_{24});$$

$$m_{66}=O\times R\times(\frac{13}{35}\overline{m}_{pile}L+B_{33});$$

$$m_{67}=O\times R\times(\frac{-11}{210}\overline{m}_{pile}L^2+B_{34});$$

$$m_{77}=O\times R\times(\frac{1}{105}\overline{m}_{pile}L^3+B_{44});\ \overline{m}_{pier}=A_{pier}\rho_{pier};$$

$$\overline{m}_{pile}=A_{pile}\rho_{pile}$$

where

$$B=A_{pile}\rho_s\alpha_m\begin{bmatrix}\frac{13L}{35} & \frac{11L^2}{210} & \frac{9L}{70} & \frac{-13L^2}{420}\\ & \frac{L^3}{105} & \frac{13L^2}{420} & \frac{-L^3}{140}\\ & & \frac{13L}{35} & \frac{-11L^2}{210}\\ sym. & & & \frac{L^3}{105}\end{bmatrix} \quad (A4)$$

The damping matrix of the bridge system (Fig. 3) is

$$C_{system}=\begin{bmatrix}c_{11} & c_{12} & c_{13} & c_{14} & c_{15} & c_{16} & c_{17}\\ & c_{22} & c_{23} & c_{24} & c_{25} & c_{26} & c_{27}\\ & & c_{33} & c_{34} & c_{35} & c_{36} & c_{37}\\ & & & c_{44} & c_{45} & c_{46} & c_{47}\\ & & & & c_{55} & c_{56} & c_{57}\\ & sym. & & & & c_{66} & c_{67}\\ & & & & & & c_{77}\end{bmatrix} \quad (A5)$$

In which

Rayleigh damping for structural components:

$$c_{ij}=\alpha\times m_{ij}+\beta\times k_{ij};\forall i=1,2,3\ \&\ j=1,2,3$$

For soil-pile elements:

$$c_{ij}=\alpha\times(m_{ij})+\beta\times(k_{ij})+C_{pq}; \quad (A6)$$

$$\forall i=4,5,6,7\ \&\ j=4,5,6,7;\ p=i-3;q=j-3$$

$$\begin{Bmatrix}\alpha\\ \beta\end{Bmatrix}=\frac{2\xi}{\omega_1+\omega_2}\begin{Bmatrix}\omega_1\omega_2\\ 1\end{Bmatrix}$$

where α and β are Rayleigh damping coefficients and

For the uniform case (n=0):

$$C=\pi d\rho_s\alpha_c V_{sd}\begin{bmatrix}\frac{13L}{70} & \frac{11L^2}{420} & \frac{9L}{140} & \frac{-13L^2}{840}\\ & \frac{L^3}{210} & \frac{13L^2}{840} & \frac{-L^3}{280}\\ & & \frac{13L}{70} & \frac{-11L^2}{420}\\ sym. & & & \frac{L^3}{210}\end{bmatrix}$$

For the proportional case (n=1):

$$C=\pi d\rho_s\alpha_c V_{sd}\begin{bmatrix}\frac{3712\,L^{1.5}}{45045\,d^{0.5}} & \frac{128\,L^{2.5}}{9009\,d^{0.5}} & \frac{2008\,L^{1.5}}{45045\,d^{0.5}} & \frac{-464\,L^{2.5}}{45045\,d^{0.5}}\\ & \frac{128\,L^{3.5}}{45045\,d^{0.5}} & \frac{8L^{2.5}}{715\,d^{0.5}} & \frac{-16\,L^{3.5}}{6435\,d^{0.5}}\\ & & \frac{347\,L^{1.5}}{2145\,d^{0.5}} & \frac{-46\,L^{2.5}}{2145\,d^{0.5}}\\ sym. & & & \frac{8L^{3.5}}{2145\,d^{0.5}}\end{bmatrix} \quad (A7)$$

For the parabolic case (n=0.5):

$$C=\pi d\rho_s\alpha_c V_{sd}\begin{bmatrix}\frac{135168\,L^{1.25}}{1121575\,d^{0.25}} & \frac{192512\,L^{2.25}}{10094175\,d^{0.25}} & \frac{59712\,L^{1.25}}{1121575\,d^{0.25}} & \frac{-2816\,L^{2.25}}{224315\,d^{0.25}}\\ & \frac{4096\,L^{3.25}}{1121575\,d^{0.25}} & \frac{3392\,L^{2.25}}{258825\,d^{0.25}} & \frac{-256\,L^{3.25}}{86275\,d^{0.25}}\\ & & \frac{878\,L^{1.25}}{5075\,d^{0.25}} & \frac{-24\,L^{2.25}}{1015\,d^{0.25}}\\ sym. & & & \frac{64\,L^{3.25}}{15225\,d^{0.25}}\end{bmatrix}$$

where $V_{sd}=\sqrt{G_{sd}/\rho_s}$ (A8)